Adaptive multi-sample-based photoacoustic tomography with imaging quality optimization

Yuxin Wang (王育昕)[1], Jie Yuan (袁 杰)[1,*], Sidan Du (都思丹)[1], Xiaojun Liu (刘晓峻)[2], Guan Xu (徐 冠)[3], and Xueding Wang (王学鼎)[3,]**

[1]*School of Electronic Science and Engineering, Nanjing University, Nanjing 210093, China*
[2]*School of Physics, Nanjing University, Nanjing 210093, China*
[3]*Department of Radiology, University of Michigan, Ann Arbor, MI 48109, USA*
**Corresponding author: yuanjie@nju.edu.cn; **corresponding author: xdwang@umich.edu*
Received November 28, 2014; accepted March 26, 2015; posted online May 18, 2015

The energy of light exposed on human skin is compulsively limited for safety reasons which affects the power of photoacoustic (PA) signal and its signal-to-noise ratio (SNR) level. Thus, the final reconstructed PA image quality is degraded. This Letter proposes an adaptive multi-sample-based approach to enhance the SNR of PA signals and in addition, detailed information in rebuilt PA images that used to be buried in the noise can be distinguished. Both *ex vivo* and *in vivo* experiments are conducted to validate the effectiveness of our proposed method which provides its potential value in clinical trials.

OCIS codes: 100.2980, 170.1065, 170.5120.
doi: 10.3788/COL201513.061001.

Research on photoacoustic tomography (PAT) got prosperous development for its being promisingly characterized with noninvasive and nonionizing diagnose of breast cancer, arthritis, and relevant disease. PAT combines the metrics of both ultrasound imaging and pure optical imaging technique, providing high ultrasonic resolution and high optical contrast images[1–5]. Due to the peculiarity that the optical absorption characteristic of blood has a strong relationship with the hemoglobin content, functional imaging as well as structural imaging can also be realized by PAT, making this imaging modality extremely potential in clinical application[6].

The basic principle of PAT is that a tissue is irradiated with short nanosecond laser pulses, and then the absorbed energy may result in a thermo-elastic expansion and subsequent contraction of irradiated volume that generates time-trace photoacoustic (PA) waves, which can be acquired by scanning small-aperture ultrasound detectors over a surface that encloses the source under study. The recorded PA wave can then be reconstructed to spatially resolve the initial absorber distribution and concentration via PA reconstruction algorithms[7–9]. However, biomedical tissue is a highly scattering medium for electromagnetic waves in the optical spectral range, and the propagation ultrasound waves are extremely attenuated before received by ultrasound sensors. Furthermore, the dose of laser beam exposed on the biomedical tissue has to be limited under 20 $\mathrm{mJ/cm^2}$ for safety operation. Thus, in clinical trials, ultrasound transducer can only receive weak PA signals with low signal-to-noise ratio (SNR) which degraded the final reconstructed PA images[10–14]. This Letter proposes an adaptive multi-sample-based approach to enhance the SNR of PA signals and in addition, detailed information of PAT that used to be buried in the noise and artifacts can be distinguished.

The PA reconstruction is an inverse problem of the source pressure. We assume that a tissue with inhomogeneous microwave absorption but a relatively homogeneous acoustic property and the heat diffusion's effect on the thermoacoustic wave can be ignored. For cases where the scanning radius in a circular scan configuration is much greater than the PA wavelengths, the optical absorption $p_0(r)$ within the sample at a given position r is given as[1]

$$p_0(r) = -\frac{r_0^2 \mathrm{C_p}}{2\pi c^4 \beta} \int_{\theta_0} \mathrm{d}\theta_0 \frac{1}{t} \frac{\partial p(r_0, t)}{\partial t}\bigg|_{t=|r-r_0|/c}, \tag{1}$$

where c is the speed of sound; β is the isobaric volume expansion coefficient; $\mathrm{C_p}$ is the heat capacity; r_0 is the detector position with respect to the imaging cente; $p(r_0, t)$ is the PA signals detected at each scanning angle θ_0. $\partial p(r_0, t)/\partial t$ can be calculated through inverse Fourier transform[15]

$$\frac{\partial p(r_0, t)}{\partial t} = \mathrm{FT}^{-1}\{-i\omega p(r_0, \omega)\, W_{\Omega}(\omega)\}, \tag{2}$$

where FT^{-1} donates the inverse Fourier transform; ω is angular frequency; $W_{\Omega}(\omega)$ is a window function to depress the high-frequency noise, which is characterized by a cut-off angular frequency Ω. In our work, we chose Hanning window, which has smooth edge shape and less calculation complexity

$$W_{\Omega}(\omega) = \begin{cases} 0.5 + 0.5\cos\left(\pi \frac{\omega}{\Omega}\right), & \text{if } |\omega| < \Omega \\ 0, & \text{otherwise} \end{cases}. \tag{3}$$

We can discern from Eq. (1) that the SNR of the received PA signals is of great importance to the image

quality of PAT. Normally, using single-sampled PA signal can only build a low-SNR PA image. Since the PA signal and the random noise are uncorrelated in each measurement procedure, we can apply averaging frames using multi-sample method to enhance the SNR of reconstructed PA images. However, after applying multi-sample method, with the improvement of SNR, in real biomedical tissue, the spatial resolution and detailed information of reconstructed PAT image is hardly increased (as shown in a subsequent paragraph). This abnormal phenomenon can be explained by the schematic in Fig. 1.

Due to the uncertainty accumulated by the whole experiment system, there always exists tiny time shift between different PA frames. While the interval time between two sequenced pulsed lasers is precisely fixed ($\max\{|T1-T2|\}<1$ ns), the ultrasound signals received are not perfectly aligned ($\max\{|T2-T4|\}>0.1\,\mu$s).

By calculating the cross correlation between the two PA frames $p_1(t)$ and $p_2(t)$, the time shift t_s can be determined. For continuous signals, the cross correlation is defined as

$$p_1(t) * p_2(t) = \int_{-\infty}^{\infty} p_1^*(\tau) p_2(t+\tau)\mathrm{d}\tau, \tag{4}$$

where $p_1^*(t)$ is the complex conjugation of $p_1(t)$. With the cross correlation[16], t_s can be determined according to the time offset between zero and the highest peak. For discrete signals $p_1(n)$ and $p_2(n)$, their cross correlation is

$$\hat{R}_{p_1p_2}(m) = \begin{cases} \frac{1}{L-|m|}\sum_{n=0}^{L-m-1} p_1(n+m)p_2(n) & m \geq 0 \\ \hat{R}_{p_2p_1}(-m) & m<0 \end{cases}, \tag{5}$$

where L is the maximum length of signal $p_1(n)$ and $p_2(n)$. However, using Eq. (5) can only get a maximal precision of shift time n_s between $p_1(n)$ and $p_2(n)$ at $1/f_{\text{sample}}$, where f_{sample} is the sample frequency of the receiving system. With N times interpolation on $p_1(n)$ and $p_2(n)$, the precision of shift time n_s will increase N times. In our work, shift time n_s is calculated by applying cubic spline interpolation[17] on receiving signals before using Eq. (5). With correct n_s, received PA signals are aligned and averaged as

$$\hat{p}(r, L_{\text{int}}) = \frac{1}{N_s}\sum_{i=1}^{N_s} p_{i\_\text{shift}}(r, L_{\text{int}}), \tag{6}$$

where L_{int} is the interpolated length of PA signal; N_s is the number of sampled frames; $p_{i\_\text{shift}}(r, L_{\text{int}})$ are the shifted PA frames. Finally, N times sample is applied on $\hat{p}(r, L_{\text{int}})$ to generate PA signal $\hat{p}(r, n)$ for imaging

$$\hat{p}(r, n) \equiv \hat{p}(r, L_{\text{int}})|_{L_{\text{int}}=nN}. \tag{7}$$

Our experiment system integrates a tunable optical parametric oscillator laser (Vibrant B, Opotek Inc., Carlsbad, CA, USA) pumped by the second harmonic output of a Nd:YAG pulsed laser (Brilliant B, Quantel, Bozeman, MT, USA) as the illumination source. The laser system is turned to 720 nm which gives the maximum output energy of 60 mJ/pulse. The pulsed laser beam with a repetition rate of 10 Hz and pulse width of 5.5 ns illuminates the imaging domain. A Verasonics system (Model V3, Redmond, WA, USA) was programmed to work with a computer. To build real-time PA images, we applied our hardware-based optimization method in experiments[18]. In addition, we applied our linear delay compensation optimization method (similar to the concept of beamforming) to build full-range focused PA images[19]. The schematic diagram of the imaging system is shown in Fig. 2.

The first experiment is conducted with a phantom containing four human hairs. These hairs are fixed on a U-shaped plastic holder. A metal shank is also attached on it so as to make it submerge in water. We use the Philips CL15-7 transducer probe (liner array, 128 elements, center frequency at 9 MHz with 0.178 mm element pitch) to detect the PA signals. The probe is vertical to the hairs

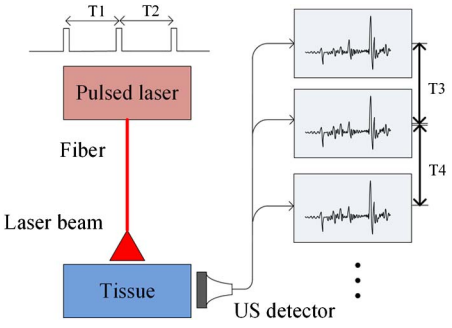

Fig. 1. Schematic of the multi-sampling procedure.

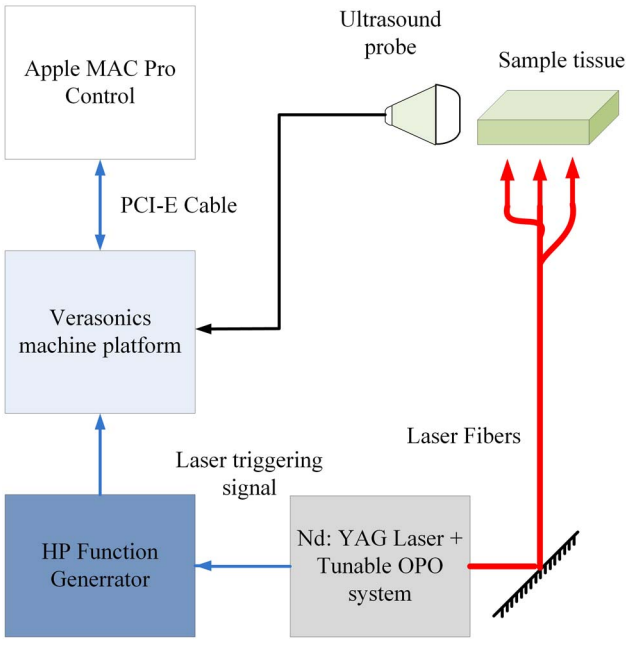

Fig. 2. Schematic diagram of the experiment system.

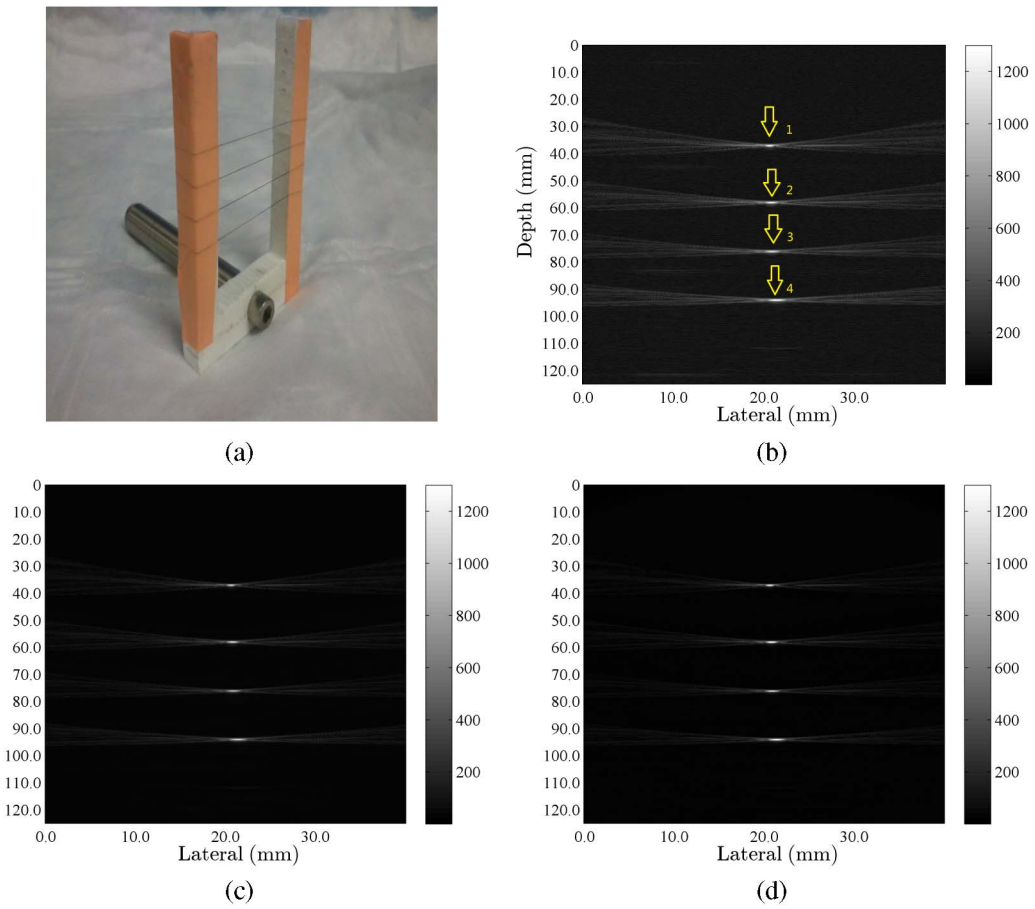

Fig. 3. Human hair phantom reconstruction: (a) Model of the phantom. (b) PA image with single sample frame. (c) PA image with traditional multi-sample-based method. (d) PA image with our multi-sample-based method.

in order to get the cross section image of the four hairs. Figure 3(a) shows the model of our phantom. Figure 3(b) is the reconstructed PA image using one sample frame which contains strong background noise and artifacts. Figures 3(c) and 3(d) are the reconstructed PA images with simple multi-frame average method and our proposed multi-frame method, respectively. Both results come from the same 10 sampled frames. In this work, we applied 3× interpolation to rectify the random shift between sample frames. It is apparent that the noise and artifacts in Fig. 3(d) is effectively depressed and the four human hair sections can be easily discerned from the background.

To quantify the effect of our method, we compare the peak SNR (PSNR; as shown in Table 1) of the reconstructed PA images. For all four human hairs, when computing their PNSRs, the background is set to a 50 pixels × 50 pixels region far away from the region of interest. In Table 1, PNSR_S is the PSNR of the PA image reconstructed using one sample frame, PSNR_N is the PSNR of the PA image reconstructed using simple multi-sample averaging method, and PSNR_M is the PSNR of the PA image reconstructed using our multi-sample-based approach. From Table 1 we can see that 6 dB quality improvement is achieved after applying our proposed method.

Table 1. PSNR Improved with Multi-Sample-Based Approach

Hair No.	1	2	3	4
PSNR_S (dB)	58.6098	59.2684	56.7737	59.4863
PSNR_N (dB)	62.8133	63.1143	60.4926	63.0089
PSNR_M (dB)	64.4487	65.5755	62.9599	65.3259

Another experiment is conducted with a volunteer's index finger, which is fixed to avoid moving artifacts in the process of PAT. The laser beam is parallel to the finger while vertical to the CL15-7 probe. Figure 4(a) is

Table 2. PSNR Comparison between Different Approaches

Region	One-Sample-Based Method	Simple Multi-Sample-Based Method	Our Method
A	36.5235	43.3422	46.4543
B	33.3890	41.9003	44.0908
C	35.7781	43.0783	45.6740

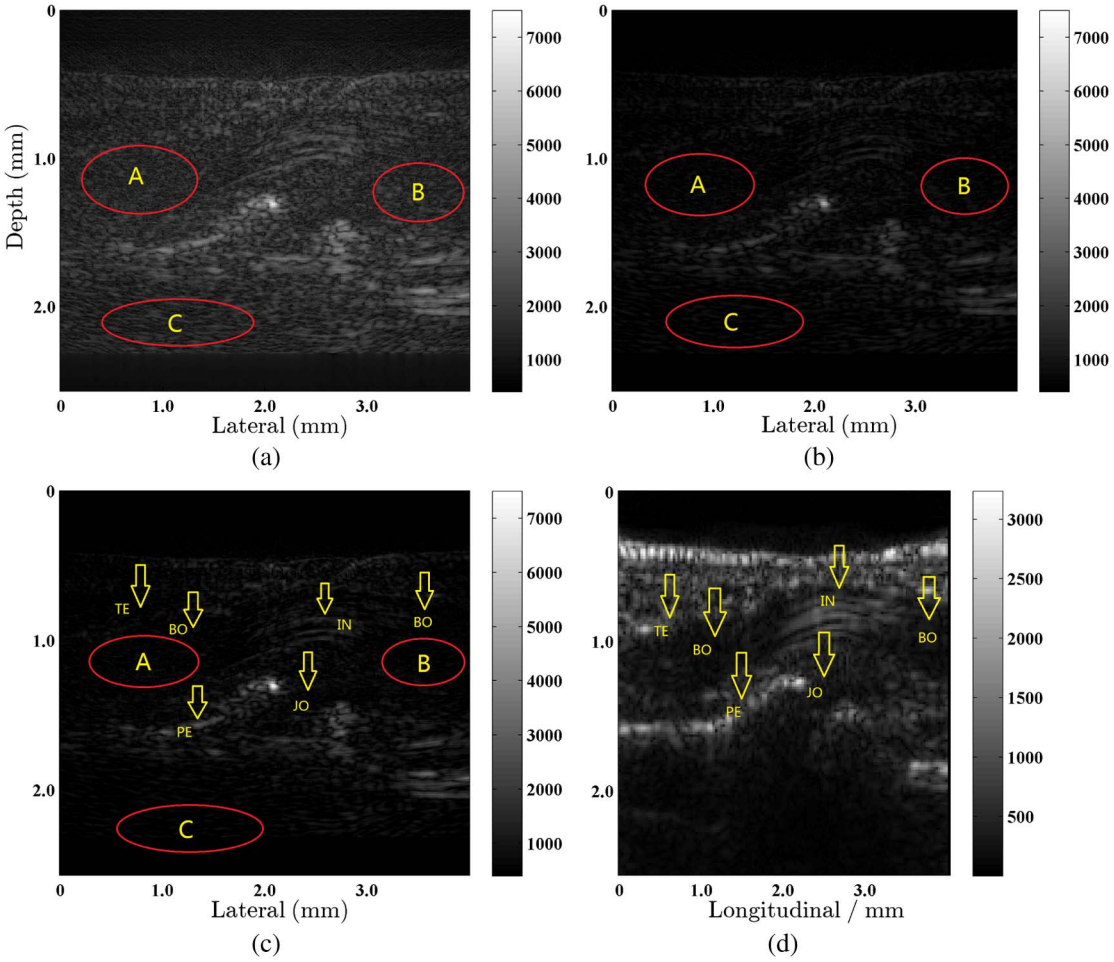

Fig. 4. Images of human index finger joint: (a) PA image using one sample frame. (b) PA image using simple multi-frames average method. (c) PA image using our proposed multi-frame-based method. (d) B-mode ultrasound image; BO, bone; IN, inner structure of tendon; JO, joint; PE, periosteum; TE, tendon.

the reconstructed PA image using one sample frame. Figures 4(b) and 4(c) are the reconstructed PA images of the same target using simple multi-frame average method and our proposed method, respectively. We can see that, as a whole, Fig. 4(b) presents better image quality than Fig. 4(a) especially in the regions where we mark in the colored line (Regions A–C). Figure 4(c) is even better than Fig. 4(b) in presenting clear infrastructures. To quantify the quality of reconstructed PA images, PSNR comparison among different methods is listed in Table 2 which indicates that our proposed method has overwhelming advantages over other ones. Furthermore, we additionally include a B-mode ultrasound image [shown as Fig. 4(d)] of the same target for comparison. This *in vivo* experiment proves that reconstructed PA image with our proposed method strictly match the biomedical infrastructure (tendon, bone, joint, periosteum, and inner structure of tendon) to those in ultrasound image. To enhance the noise and artifacts, these images are displayed using nonlinear gray level.

In conclusion, we adaptively utilize repeatedly sampled PA signals to yield optimized biomedical PA images which not only suppress the noise and artifacts, but also enhance the detailed information in reconstructed images. We hope our improved multi-sample-based approach will benefit future clinical trials and other *in vivo* research.

This work was supported by the National Natural Science Foundation of China (No. 61201425), the Natural Science Foundation of Jinagsu Province (No. BK20131280), and the Priority Academic Program Development of Jiangsu Higher Education Institutions.

References

1. X. Wang, Y. Pang, G. Ku, X. Xie, G. Stoica, and L. V. Wang, Nat Biotechnol. **21**, 803 (2003).
2. L. V. Wang and S. Hu, Science **335**, 1458 (2012).
3. S. Mallidi, G. P. Luke, and S. Emellianov, Trends Biotechnol. **29**, 213 (2011).
4. P. Beard, Interface Focus **1**, 602 (2011).
5. D. Piras, W. Xia, W. Steenbergen, T. G. V. Leeuwen, and S. Manohar, IEEE J. Sel. Top. Quantum Electron. **16**, 730 (2010).
6. J. Zhang, S. Yang, X. Ji, Q. Zhou, and D. Xing, J. Am. Coll. Cardiol. **64**, 385 (2014).
7. H. Qin, T. Zhou, S. Yang, Q. Chen, and D. Xing, Nanomedicine **8**, 1611 (2013).

8. J. Zhong, S. Yang, X. Zheng, T. Zhou, and D. Xing, Nanomedicine **8**, 903 (2013).
9. S. Tzoumas, A. Zaremba, U. Klemm, A. Nunes, K. Schaefer, and V. Ntziachristos, Opt. Lett. **39**, 3523 (2014).
10. L. Zeng, D. Xing, H. Gu, D. Yang, S. Yang, and L. Xiang, Med. Phys. **34**, 556 (2007).
11. C. Zhang and Y. Wang, Chin. Opt. Lett. **12**, 111703 (2014).
12. Z. Wu, M. Sun, Q. Wang, T. Liu, N. Feng, J. Liu, and Y. Shen, Chin. Opt. Lett. **12**, 121701 (2014).
13. R. J. Zemp, R. Bitton, M. Li, K. K. Shung, G. Stoica, and L. V. Wang, J. Biomed. Opt. **12**, 010501 (2007).
14. G. Ku and L. V. Wang, Opt. Lett. **30**, 507 (2005).
15. M. Xu and L. V. Wang, Med. Phys. **29**, 1661 (2002).
16. J. Brunker and P. Beard, J. Acoust. Soc. Am. **132**, 1780 (2012).
17. H. S. Hou and H. Andrews, IEEE Trans. Acoust. Speech Signal Process. **26**, 508 (1978).
18. T. Feng, J. Yuan, Y. Zhou, Y. Yu, and G. Xu, Chin. Phys. Lett. **30**, 100702 (2013).
19. W. Li, J. Yuan, Q. Shen, Y. Yu, Y. Zhou, S. Du, X. Liu, G. Xu, and X. Wang, Chin. Phys. Lett. **31**, 054302 (2014).